Field Measurements of Unsteady Turbulence in a Tidal Bore: the Garonne River in October 2013

David Reungoat, Lecturer, *University of Bordeaux, I2M - Laboratoire TREFLE, Pessac, France*
Email: reungoat@enscbp.fr

Hubert Chanson (IAHR Member), Professor, *School of Civil Engineering, The University of Queensland, Brisbane, Australia*

Email: h.chanson@uq.edu.au (Corresponding Author)

Claire E. Keevil, Ph.D. Research student, *University of Hull, Department of Geography, Environment and Earth Sciences, Hull HU6 7RX, United Kingdom.*
Email: c.keevil@hull.ac.uk

Full correspondence details:

The University of Queensland, School of Civil Engineering,

Brisbane QLD 4072, Australia

Tel.: (61 7) 3365 3516 - Fax: (61 7) 3365 45 99,

Email: h.chanson@uq.edu.au

ABSTRACT

A tidal bore is an unsteady rapidly-varied open channel flow generated by the swift advance of the early flood tide in a funnelled shape river estuary when the tidal range exceeds 4.5 to 6 m. This contribution presents a detailed field investigation conducted on the tidal bore of the Garonne River (France). The bore was undular and the bore's leading edge was followed by well-defined secondary waves, or whelps. The instantaneous ADV velocity data indicated large and rapid fluctuations of all velocity components during the tidal bore. Large Reynolds shear stresses were observed during and after the tidal bore passage. The investigation characterised some unusual transient turbulence caused by the bore propagation in a large river system, and the results suggested the advection of large scale eddies in the wake of the bore front. The present study highlighted the need for detailed field measurements with fine temporal resolution, to characterize the highly unsteady rapidly-varied nature of tidal bore flows.

Keywords: Acoustic Doppler velocimetry, field measurements, Garonne River, tidal bore, large-scale structures, turbulence.

1. Introduction

A tidal bore may form at the leading edge of the flood tide in an estuary, when the tidal range exceeds 4.5-6 m and the channel bathymetry amplifies the flood tidal wave (Tricker 1965, Chanson 2011). The bore is a rapidly-varied, unsteady free-surface flow characterised by a discontinuity of the water depth, and velocity and pressure fields (Lighthill 1978, Liggett1994). In an estuary, the occurrence of a tidal bore relies upon a delicate balance between the tidal amplitude, the freshwater discharge, and the river mouth and channel bathymetry. This balance may be disturbed by changes in boundary conditions and freshwater runoff; for example, a number of man-made interventions have led to the modification and sometimes disappearance of tidal bores, in France, Canada, Mexico (Chanson 2011). Bores, or positive surges, may also be observed in canals and flumes (Benet and Cunge 1971, Treske 1994). A related process is a tsunami wave propagating upriver led by a positive surge (Tanaka et al. 2012). Such tsunami-induced bores may propagate far upstream, as seen in Japan in 1983, 2001, 2003 and 2011, and during the 26 December 2004 tsunami disaster in the Indian Ocean.

During the early flood tide, the steepening of the free-surface and formation of the tidal bore may be predicted using the shallow-water equations (Stoker 1957, Liggett 1994). After inception, the front of the bore can be analysed as a hydraulic jump in translation (Lighthill 1978, Chanson 2012). Neglecting the boundary friction, the continuity and momentum principles provide an expression of the ratio of conjugate cross-section areas A_2/A_1 as a function of the tidal bore Froude number F_1:

$$\frac{A_2}{A_1} = \frac{1}{2} \frac{\sqrt{\left(2 - \frac{B'}{B}\right)^2 + 8 \frac{B'/B}{B_1/B} \mathsf{F}_1^2} - \left(2 - \frac{B'}{B}\right)}{\frac{B'}{B}} \tag{1}$$

where A_1 is the initial flow cross-section area, A_2 is the conjugate flow cross-section area immediately after the bore passage, B and B' are characteristic channel widths:

$$B = \frac{A_2 - A_1}{d_2 - d_1} \tag{2}$$

$$B' = \frac{\int_{A_1}^{A_2} \rho g (d_2 - z) \mathrm{d}A}{\frac{1}{2} \rho g (d_2 - d_1)^2} \tag{3}$$

z is the vertical distance from the bed, d_1 and d_2 are respectively the initial and new flow depths, and the Froude number F_1 is defined as:

$$\mathsf{F}_1 = \frac{V_1 + U}{\sqrt{g \frac{A_1}{B_1}}} \tag{4}$$

V_1 is the initial river flow velocity positive downstream, U is the bore celerity positive upstream, g is the gravity acceleration, B_1 is the initial free-surface width (Chanson 2012). For a bore in a rectangular prismatic channel, Equation (1) yields to the classical Bélanger equation (Bélanger 1841, Liggett1994).

In the present study, new field measurements were conducted during the tidal bore of the Garonne River (France) on 19 October 2013. The free-surface properties were compared with the re-analysis of previous field data sets (Table 1). The instantaneous velocity measurements were performed continuously at high frequency (200 Hz) prior to, during and after the tidal bore. It is the aim of this contribution to simultaneously characterise the unsteady water elevation and velocity field, including the Reynolds stresses.

2. Site study and instrumentation

The Garonne River, France experiences a tidal bore in the region between Bordeaux and for the next 50 km upstream (Fig. 1). Field measurements were conducted in the Arcins Channel of the Garonne River, between Arcins Island and the eastern bank, about 6.5 km south-west of the centre of the City of Bordeaux (Fig. 2). The Arcins channel is 1.8 km long, 70 m wide and about 1.1 to 2.5 m deep at low tide. Figure 1a shows the tidal bore entering the Arcins Channel and Figure 2b shows a surveyed cross-section, with the vertical elevation in m NGF IGN 1969, where NGF IGN stands for Nivellement Général de la France by the Institut Géographique National. The field study was conducted under spring tide conditions in the afternoon of 19 October 2013, at the site used by Chanson et al. (2011) and Reungoat et al. (2014a). The tidal range was 6.09 m and the tidal cycles presented some diurnal inequality on 19 October 2013. The measurements commenced during the ebb tide prior to the passage of the bore and were conducted continuously for a further 1.5 h after the bore. Further information on the field study and data were reported in Reungoat et al. (2014b).

The free surface elevation was measured manually using a survey staff; during the bore front passage, it was recorded using a video camera at 25 fps. The survey staff was mounted 2 m from the acoustic Doppler velocimeter (ADV), to minimize any interference with the sampling volume. The instantaneous velocity components were recorded with a Nortek[TM] ADV Vectrino+ (10 MHz, serial number VNO1356). The ADV system was equipped with a down-looking head (Field probe) equipped with four receivers. The ADV was

mounted vertically 0.98 m below the surface, beneath the hull of a heavy and sturdy pontoon. Figure 2 illustrates the ADV sampling volume location in the surveyed cross-section at the end of the ebb tide. Herein the velocity range was 2.5 m s^{-1}, and the ADV setup included a transmit length of 0.3 mm and a sampling volume of 1.5 mm height. The ADV was sampled continuously at 200 Hz. All ADV data underwent a post-processing procedure to eliminate any erroneous or corrupted data, using the software WinADV^{TM} version 2.028. The post-processing included the removal of communication errors, the removal of average signal to noise ratio (SNR) data less than 5 dB, the removal of average correlation values less than 60% following McLelland and Nicholas (2000) and despiking using the phase-space thresholding technique developed by Goring and Nikora (2002). The percentage of good samples was superior to 82% for the entire data set.

3. Flow patterns and bore properties

The tidal bore formed at the northern end of the Arcins channel, extending across the entire width (Fig. 1a). During its upstream propagation, the bore was undular, including at the sampling location, but changed shape rapidly in response to local channel bathymetry. The bore front was well marked (e.g. by the surfers seen in Fig. 1a) and it was followed by a series of undulations (or whelps) lasting for a few minutes, with a wave period of about 1 s. The free-surface elevation rose very rapidly by 0.3 m in the first 10-15 s and by further 1.1 m during the next 60 s (Fig. 3). Figure 3 shows the water elevation data at Arcins and Bordeaux, the latter gauge being located 10 km downstream of the Arcins Channel and shown in Figure 2a. The passage of the tidal bore on 19 October 2013 is clearly seen in Figure 3 and the data are further compared with surface velocity measurements in the centre of the Arcins Channel.

The tidal bore front corresponded to a marked rise in free-surface elevation. The Froude number was calculated based upon the surveyed channel cross-section and field observations yielding $F_1 = 1.27$ (Table 1), which was consistent with the undular nature of the bore. The present observations are reported in Figure 4 in terms of the ratio of conjugate cross-sectional areas A_2/A_1 as a function of the Froude number. The present data (red star symbol) are compared with the momentum principle solution (Eq. (1)) (open circles) and previous field data (Table 1) (Fig. 4). For comparison, the classical Bélanger equation, developed for a smooth rectangular channel, is also shown:

$$\frac{d_2}{d_1} = \frac{1}{2}\left(\sqrt{1 + 8 F_1^2} - 1\right) \tag{5}$$

Figure 4 indicates a good agreement between Equation (1) and tidal bore field data, demonstrating the limitations of the Bélanger equation (1) in natural channels. Our result, although close to the Bélanger equation, is similar to all the results from previous studies by considering the measurement accuracy. The full data sets are reported in a tabular format in Table 1.

The passage of the undular bore was followed with a rapid rise in water elevation ($t = 61512$ s in Fig. 3) and some marked secondary wave motion behind the front. A key feature was the smooth bore front followed by free-surface undulations, a feature of undular bores previously documented in the field (Wolanski et al. 2004, Chanson et al. 2011). The dimensionless undulation characteristics are shown in Figure 5: i.e., the wave length and wave steepness. In Figure 5, the present observations are compared to field and laboratory data of undular bores, as well as to analytical solutions based upon the linear wave theory and Boussinesq equations (Lemoine 1948, Andersen 1978). The dimensionless wave length $L_w/(A_1/B_1)$ decreased with increasing Froude number and the data were relatively close to a solution of the Boussinesq equation (Fig. 5a). The undulation wave steepness a_w/L_w increased with increasing Froude number up to $F_1 = 1.3$ (Fig. 5b). For larger Froude numbers, the wave steepness was restricted by the appearance of some breaking at the first wave crest and the data tended to decrease with increasing Froude number for $F_1 > 1.3$. In Figure 5, the present data (red star symbol) showed comparable trends with previous observations, despite the irregular bathymetry of the natural channel.

4. Instantaneous velocity and turbulent stress data

The instantaneous velocity components were measured continuously prior to, during and after the undular tidal bore. Figure 6 shows the velocity data about the time of passage of the bore front, with the longitudinal velocity component V_x positive downstream, the transverse velocity component V_y positive towards Arcins

Island, and the vertical velocity component V_z positive upwards. The water depth measurements are also included in Figure 6.

For the last two hours of the ebb tide the current velocity dropped from +0.6 m s^{-1} down to +0.1 m s^{-1} (Fig. 3 & 6). The passage of the tidal bore (t = 61512 s, Fig. 6) induced a marked effect on the velocity field and water depth. The main current reversed its direction almost immediately and the mean longitudinal velocity ranged typically between -0.8 and -1.2 m s^{-1} after the bore passage, where the negative sign reflected the upriver flow direction. The bore passage induced strong mixing in the channel; although the free-surface ahead of the first wave crest appeared smooth, intense mixing was observed at the water surface next to the banks when the bore arrived. The bore passage was associated with loud crashes of waters on the pontoons, boat ramps and banks.

During the bore passage, the mean longitudinal flow deceleration was -0.18 m s^{-2}, or -0.02×g. The tidal bore front was characterized by large fluctuations of all velocity components (Fig. 6). The longitudinal velocity component fluctuated between -0.6 to -1.35 m s^{-1} after the passage of the bore, the transverse velocities ranged from -0.2 to +0.35 m s^{-1}, while the vertical velocity data fluctuated between -0.3 and +0.1 m s^{-1}. The vertical velocity data showed some oscillations with period about 1 to 1.5 s immediately after the bore passage: i.e., 61520 < t < 61555 s in Figure 6. It is believed that these oscillations were closely linked with the free-surface undulations, or whelps, and their induced vertical motion. The irrotational flow theory predicts a redistribution of both longitudinal and vertical velocities between wave crests and troughs, with the same periodicity as the free-surface elevation but out of phase (Rouse 1938, Montes and Chanson 1998). This pattern would be consistent with the present observations and was previously documented in laboratory tidal bores (Koch and Chanson 2008, Chanson 2010).

The turbulent properties were estimated during the late ebb tide and early flood tide including for the tidal bore passage. Herein the turbulent velocity fluctuation v was the deviation of the instantaneous velocity V from a 'mean' value, which was the low-pass filtered value, or variable interval time average VITA, calculated using a threshold frequency of 2 Hz (Reungoat et al. 2014b). The threshold frequency was selected between the free-surface undulation frequency ($1/T_w$) and twice the undulation frequency ($2/T_w$) based upon a sensitivity analysis, following earlier works (Chanson et al. 2011, Chanson and Docherty 2012). Some basic turbulence characteristics are summarised in Tables 2 and 3, in terms of the dimensionless velocity fluctuations and integral time scales. Although the velocity fluctuations were larger in the late ebb tide, the dimensionless fluctuations $v_x'/|\overline{V_x}|$, $v_y'/|\overline{V_x}|$ and $v_z'/|\overline{V_x}|$ were of similar magnitude before and after the bore passage, although smaller after the bore, where v_x', v_y' and v_z' are the standard deviations of the longitudinal, transverse and vertical velocity components respectively, and $|\overline{V_x}|$ is the amplitude of the mean longitudinal velocity component. The horizontal turbulence ratio v_y'/v_x' was equal to 0.7-0.8 before and after the bore (Table 2), with values comparable to laboratory observations in straight prismatic rectangular channels (v_y'/v_x' = 0.5-0.7, Nezu and Nakagawa 1993). The vertical turbulence ratio v_z'/v_x' was about 0.4-0.5 (Table 2): i.e., similar to the observations of Shiono and West (1987) and Trevethan et al. (2008) in estuaries, and Nezu and Nakagawa (1993) and Xie (1998) in laboratory open channels. Note that v_z'/v_y' was approximately two-thirds, implying some turbulence anisotropy. The integral turbulent time scales of each velocity component represented a measure of the longest connection in the turbulent behaviour of that velocity component. The experimental data showed some differences between before and after the bore (Table 3). The integral time scale of the longitudinal velocity component was on average 10 times larger after than before the bore passage. Reungoat et al. (2014a) reported a similar observation, which is believed to be linked to the production and advection of large eddies behind the bore, as shown by numerical models (Furuyama and Chanson 2010, Lubin et al. 2010). The integral times scales in terms of the transverse and vertical velocities were of the same order of magnitude before and after the bore (Table 3).

4.1. *Turbulent Reynolds stresses*

A Reynolds stress is proportional to the cross-product of turbulent velocity fluctuation v, where v is the deviation of the instantaneous velocity V from the VITA value (see above). The method was applied to all velocity components and the turbulent Reynolds stresses were calculated from the high-pass filtered signals. Typical results are presented in Figure 7.

The field observations showed large turbulent shear stresses, and large and rapid fluctuations in shear stresses during and after the tidal bore, for all Reynolds stress tensor components. The data indicated that the

turbulent shear stresses were significantly larger in the wake of the tidal bore (Fig. 7). Maximum instantaneous shear stress amplitudes of up to 80 Pa were recorded during and after the bore passage. The data indicated that the tidal bore likely scoured the channel bed and advected into suspension the bed material and washload upstream, behind the bore front. This was consistent with visual observations of sediment flocs bursting at the free-surface during the early flood tide. The sediment scour and advection processes applied to a significant length of the estuarine section of the Garonne River and would mobilise an enormous amount of sediments.

5.   Discussion

The field measurements demonstrated large instantaneous velocity fluctuations and turbulent stresses during the tidal bore. The instantaneous velocity fluctuations (v_x, v_y, v_z) followed relatively closely a normal distribution. The longitudinal velocity fluctuation data are plotted in Figure 8, in the form of the probability distributions functions measured before, during and immediately after the bore passage. Data were sampled in 1 cm s^{-1} bin intervals in Figure 8. For all velocity fluctuations, the skewness ranged between 0.11 and 0.23 prior to the tidal bore and between 0.06 and 0.58 during the early ebb tide. Such values are comparable to skewness measurements in turbulent open channel flows and outer boundary layer flows (Nakagawa and Nezu 1977). The excess kurtosis was between 2.5 and 4 for the v_x and v_z components, and between 0.2 and 0.3 for v_y, during both the late ebb and early flood tides.

While a turbulent flow is typically characterised by its statistical moments, a key feature is the turbulent events often associated with coherent flow structures such as eddies and bursting (Kline et al. 1967, Adrian and Marusic 2012). Turbulent event analyses were successfully applied to laboratory open channel flows (Nakagawa and Nezu 1977), atmospheric boundary layer flows (Narasimha et al. 2007) and even estuarine flows (Trevethan and Chanson 2010). However they have been rarely applied to unsteady rapidly-varied estuaries. Herein the simultaneous longitudinal and vertical velocity fluctuations, v_x and v_z respectively, were analysed into four quadrants to evaluate the contributions of the ejections and sweeps to the Reynolds stress, following Nakagawa and Nezu (1977). The four quadrants are typically called outward interaction ($v_x > 0$, $v_z > 0$), ejection ($v_x < 0$, $v_z > 0$), inward interaction ($v_x < 0$, $v_z < 0$) and sweep ($v_x > 0$, $v_z < 0$) (Nezu and Nakagawa 1993). The Reynolds stress fluctuations were investigated by using the conditional sampling method: $|v_x v_z| > H$ where H is the hole size. The contribution to $v_x v_z$ from the hole would represent the contribution during the more quiescent periods, while the second and fourth quadrants corresponded to the burst and sweep events. The field measurement results are shown in Figures 9. The fraction of the total time that $v_x v_z$ spent in the hole region is also included in Figure 9. During the late ebb tide flow (Fig. 9a), the results were comparable to steady turbulent boundary layer data. For a large proportion of time, the turbulent stress $v_x v_z$ was small. The largest contribution came from the second quadrant (burst), and the second largest contribution was the fourth quadrant (sweep). In contrast, the results during the early flood tide (Fig. 9b) indicated much larger turbulent stresses $v_x v_z$, with a lesser proportion of no-event for a given hole size. Further the proportion of time and contribution of all four quadrants were of comparable magnitude. The findings would be consistent with the observations that the early flood flow was dominated by large-scale structures generated in the wake of the bore. The interactions of these very large eddies with the free-surface were seen by all field work participants in the form of large boils and surface scars.

6.   Conclusion

During a field study in the Garonne River's tidal bore, the water elevation and instantaneous velocity field was documented prior to and during the bore event with a fine temporal resolution. The tidal bore was undular and its Froude number was $\mathsf{F}_1 = 1.27$. The bore's leading edge was followed by well-defined whelps with a wave period of about 1 s, while the wave amplitude and length were comparable to theoretical estimates and earlier field observations. The instantaneous ADV velocity data indicated large and rapid fluctuations of all velocity components. Large Reynolds shear stresses were observed during and after the tidal bore. The integral time scale and quadrant analysis results indicated some marked difference between the late ebb tide and the early flood tide flow motion immediately behind the bore. In particular the field observations suggested the upstream advection of large scale vortical structures in the wake of the bore.

The present study highlights the need for further detailed field measurements, including for the validation of any kind of modelling. A major challenge is the highly unsteady rapidly-varied nature of tidal bore flows, implying a fine temporal resolution. Altogether the field study indicated that tidal bores and positive surges in rivers and canals can generate some very intense mixing and a complex velocity field beneath the smooth free-surface. The large turbulent stresses may lead to sediment scour and suspension, impacting onto the sediment processes, water quality and ecology of the waterway. These aspects are rarely considered in numerical and laboratory models, although an accurate representation of the flow physics is critical to the advancement of science and engineering.

7. Acknowledgements

Notation

A = cross-section area (m^2)
A_1 = inflow cross-section area (m^2)
A_2 = conjugate cross-section area (m^2)
a_w = wave amplitude (m)
B = channel width (m)
B' = characteristic channel width (m)
B_1 = inflow free-surface width (m)
d = water depth (m)
d_1 = inflow depth (m)
d_2 = conjugate flow depth (m)
F_1 = Froude number (-)
g = gravity acceleration (m s^{-2})
H = hole size (m^2 s^{-2});
L_w = wave length (m)
T_{Vx} = integral time scale of longitudinal velocity component (s)
T_{Vy} = integral time scale of transverse velocity component (s)
T_{Vz} = integral time scale of vertical velocity component (s)
T_w = wave period (s)
t = time (s)
U = bore celerity (m s^{-1}) positive upstream
V_x = longitudinal velocity component (m s^{-1})
V_y = tranverse velocity component (m s^{-1})
V_z = vertical velocity component (m s^{-1})
V_1 = inflow velocity (m s^{-1})
v = velocity fluctuation (m s^{-1})
v_x = longitudinal velocity fluctuation (m s^{-1})
v_y = transverse velocity fluctuation (m s^{-1})
v_z = vertical velocity fluctuation (m s^{-1})
v_x' = longitudinal velocity fluctuation root mean square (m s^{-1})
v_y' = transverse velocity fluctuation root mean square (m s^{-1})
v_z' = vertical velocity fluctuation root mean square (m s^{-1})
x = longitudinal coordinate positive downstream (m)

REUNGOAT, D., CHANSON, H., and KEEVIL, C.E. (2015). "Field Measurements of Unsteady Turbulence in a Tidal Bore: the Garonne River in October 2013." *Journal of Hydraulic Research*, IAHR, Vol. 53, No. 3, pp. 291-301 (DOI: 10.1080/00221686.2015.1021717) (ISSN 0022-1686).

y = transverse coordinate positive towards Arcins Island (m)
z = vertical coordinate positive upstream (m)
ρ = water density (m^3 s^{-1})

References

Adrian, R.J., & Marusic, I. (2012). Coherent Structures in Flow over Hydraulic Engineering Surfaces. *J. Hydraulic Res.*, 50, 451-464. doi: 10.1080/00221686.2012.729540

Andersen, V.M. (1978). Undular Hydraulic Jump. *J. Hydraul. Div.: Proc. ASCE*, 104 (HY8), 1185-1188.

Bélanger, J. B. (1841). Notes sur l'hydraulique. [Notes on hydraulic engineering.] Ecole Royale des Ponts et Chaussées, Paris, France, session 1841–1842, 223 pages (in French).

Benet, F., & Cunge, J.A. (1971). Analysis of Experiments on Secondary Undulations caused by Surge Waves in Trapezoidal Channels. *J. Hydraulic Res.*, 9 , 11-33.

Chanson, H. (2010). Unsteady Turbulence in Tidal Bores: Effects of Bed Roughness. *J. Waterw. Port Journal of Waterway, Port, Coastal and Ocean Engineering - ASCE*, 136, 247-256. doi: 10.1061/(ASCE)WW.1943-5460.0000048

Chanson, H. (2011). *Tidal Bores, Aegir, Eagre, Mascaret, Pororoca: Theory and Observations*. Singapore: World Scientific.

Chanson. H, (2012). Momentum Considerations in Hydraulic Jumps and Bores. *J. Irrig. Drain E-ASCE*, 138, 382-385. doi: 10.1061/(ASCE)IR.1943-4774.0000409

Chanson, H., & Docherty, N.J. (2012). Turbulent Velocity Measurements in Open Channel Bores. *Eur J. Mech. B-Fluid*, 32, 52-58. Doi: 10.1016/j.euromechflu.2011.10.001

Chanson, H., Reungoat, D., Simon, B., & Lubin. P, (2011). High-Frequency Turbulence and Suspended Sediment Concentration Measurements in the Garonne River Tidal Bore. *Estuar. Coast Shelf Sc.*, 95, 2-3, 298-306. doi: 10.1016/j.ecss.2011.09.012

Furgerot, L., Mouazé, D., Tessier, B., Perez, L., & Haquin, S. (2013). Suspended Sediment Concentration in Relation to the Passage of a Tidal Bore (Sée River Estuary, Mont Saint Michel, NW France). *Proc. Coastal Dynamics 2013, Arcachon, France, 24-28 June*, 671-682.

Furuyama, S., & Chanson, H. (2010). A Numerical Solution of a Tidal Bore Flow. *Coastal Eng. Journal*, 52, 215-234. doi: 10.1142/S057856341000218X

Goring, D.G., & Nikora, V.I. (2002). Despiking Acoustic Doppler Velocimeter Data. *J. Hydraul. Eng-ASCE*, 128, 117-126. doi: 10.1061/(ASCE)0733-9429(2002)128:1(117)

Kline, S.J., Reynolds, W.C., Schraub, F.A., & Rundstadler, P.W. (1967). The Structure of Turbulent Boundary Layers. *J. Fluid Mech.*, 30, 741-773.

Koch, C., & Chanson, H. (2008). Turbulent Mixing beneath an Undular Bore Front. *J. Coastal Res.*, 24, 999-1007. doi: 10.2112/06-0688.1

Lemoine, R. (1948). Sur les Ondes Positives de Translation dans les Canaux et sur le Ressaut Ondulé de Faible Amplitude. [On the Positive Surges in Channels and on the Undular Jumps of Low Wave Height.] Jl La Houille Blanche, 183-185.

Liggett, J.A. (1994). *Fluid Mechanics*. New York, NY: McGraw-Hill.

Lighthill, J. (1978). *Waves in Fluids*. Cambridge: Cambridge University Press.

Lubin, P., Chanson, H., & Glockner, S. (2010). Large Eddy Simulation of Turbulence Generated by a Weak Breaking Tidal Bore. *Environ. Fluid Mech.*, 10 , 587-602. doi: 10.1007/s10652-009-9165-0

McLelland, S.J., & Nicholas, A.P. (2000). A New Method for Evaluating Errors in High-Frequency ADV Measurements. *Hydrol. Process.*, 14, 351-366. doi: 10.1002/(SICI)1099-1085(20000215)14:2<351::AID-HYP963>3.0.CO;2-K

REUNGOAT, D., CHANSON, H., and KEEVIL, C.E. (2015). "Field Measurements of Unsteady Turbulence in a Tidal Bore: the Garonne River in October 2013." *Journal of Hydraulic Research*, IAHR, Vol. 53, No. 3, pp. 291-301 (DOI: 10.1080/00221686.2015.1021717) (ISSN 0022-1686).

Montes, J.S., & Chanson, H. (1998). Characteristics of Undular Hydraulic Jumps. Results and Calculations. *Jl Hydraulic Engrg*, ASCE, 124(2), 192-205.

Mouazé, D., Chanson, H., & Simon, B. (2010). *Field Measurements in the Tidal Bore of the Sélune River in the Bay of Mont Saint Michel (September 2010)* Hydraulic Model Report No. CH81/10, School of Civil Engineering, The University of Queensland. Brisbane, Australia.

Nakagawa, H., & Nezu, I. (1977). Prediction of the Contribution of the Reynolds Stress from Bursting Events in Open-Channel Flows. *J. Fluid Mech.*, 80, 99-128.

Narasimha, R., Rudra Kumar, S., Prabhu, A., & Kailas, S.V. (2007). Turbulent Flux Events in a Nearly Neutral Atmospheric Boundary Layer. *Philos. T. R. Soc. A*, 365, 841–858. doi: 10.1098/rsta.2006.1949

Nezu, I., & Nakagawa, H. (1993). Turbulence in Open-Channel Flows. IAHR Monograph, IAHR Fluid Mechanics Section, Balkema Publ., Rotterdam, The Netherlands, 281 pages.

Reungoat, D., Chanson, H., & Caplain, B. (2014a). Sediment Processes and Flow Reversal in the Undular Tidal Bore of the Garonne River (France). *Environ. Fluid Mech.*, 14, 591–616. doi: 10.1007/s10652-013-9319-y

Reungoat, D., Chanson, H., & Keevil, C. (2014b). *Turbulence, Sedimentary Processes and Tidal Bore Collision in the Arcins Channel, Garonne River (October 2013)* Hydraulic Model Report No. CH94/14, School of Civil Engineering, The University of Queensland, Brisbane, Australia.

Rouse, H. (1938). *Fluid Mechanics for Hydraulic Engineers*. New York, NY; McGraw-Hill.

Shiono, K., & West, J.R. (1987). Turbulent Perturbations of Velocity in the Conwy Estuary. *Estuar. Coast Shelf S.*, 25, 533-553.

Simpson, J.H., Fisher, N.R., & Wiles, P. (2004). Reynolds Stress and TKE Production in an Estuary with a Tidal Bore. *Estuar. Coast Shelf S.*, 60, 619-627. doi: 10.1016/j.ecss.2004.03.006

Stoker, J.J. (1957). *Water Waves. The Mathematical Theory with Applications*. New York, NY: Interscience Publishers.

Tanaka, H., Nguyen, X.T., Umeda, M., Hirao, R., Pradjoko, E., Mano, A., & Udo, K. (2012). Coastal and Estuarine Morphology Changes Induced by the 2011 Great East Japan Earthquake Tsunami. *Coast Eng. J.*, 54 (1), paper 1250010. doi: 10.1142/S0578563412500106

Treske, A. (1994). Undular Bores (Favre-Waves) in Open Channels - Experimental Studies. *J. Hydraulic Res.*, 32, 355-370.

Trevethan, M., & Chanson, H. (2010). Turbulence and Turbulent Flux Events in a Small Estuary. *Environ. Fluid Mech.*, 10, 345-368. doi: 10.1007/s10652-009-9134-7

Trevethan, M., Chanson, H., & Brown, R. (2008). Turbulent Measurements in a Small Subtropical Estuary with Semi-Diurnal Tides. *J. Hydraul. Eng-ASCE*, 134, 1665-1670. doi: 10.1061/(ASCE)0733-9429(2008)134:11(1665)

Tricker, R.A.R. (1965). *Bores, Breakers, Waves and Wakes*. New York, NY: American Elsevier.

Wolanski, E., Williams, D., Spagnol, S., & Chanson, H. (2004). Undular Tidal Bore Dynamics in the Daly Estuary, Northern Australia. *Estuar. Coast Shelf Sc.*, 60 (4), 629-636.

Xie, Q. (1998). *Turbulent Flows in Non-Uniform Open Channels: Experimental Measurements and Numerical Modelling*. Ph.D. thesis, Dept. of Civil Eng., University of Queensland, Brisbane, Australia.

Table 1- Details of field measurements of tidal bores

Reference	River	Date	Bore type	F_1	U m s^{-1}	V_1 m s^{-1}	d_1 m	A_1 m^2	B_1 m	d_2-d_1 m	B_2/B_1	B/B_1	B'/B_1	A_2/A_1	a_w/L_w	$L_w/(A_1/B_1)$	T_w (s)
(1)	(2)	(3)	(4)	(5)	(6)	(7)	(8)	(9)	(10)	(11)	(12)	(13)	(14)	(15)	(16)	(17)	(18)
Wolanski et al. (2004)	Daly River	2/07/03	Undular	1.04	4.70	0.15	1.50	289.3	129.2	0.28	1.013	1.007	1.001	1.13	0.0009	19.89	9.48
Simpson et al. (2004)	Dee River	6/09/03	Breaking	1.79	4.1	0.15	0.72	39.3	68.3	0.45	1.066	1.030	1.085	1.80	--	--	--
Chanson et al. (2011)	Garonne River	10/09/10	Undular	1.30	4.49	0.33	1.77	105.7	75.4	0.50	1.083	1.042	1.018	1.37	0.061	3.97	1.24
		11/09/10	Undular	1.20	4.20	0.30	1.81	108.8	75.8	0.46	1.076	1.032	1.021	1.33	0.047	3.75	1.28
Mouaze et al. (2010)	Sélune River	24/09/10	Breaking	2.35	2.00	0.86	0.38	5.25	34.7	0.34	3.37	2.33	1.92	6.19	--	--	--
		25/09/10	Breaking	2.48	1.96	0.59	0.33	3.56	33.2	0.41	3.53	2.33	1.98	9.79	--	--	--
Furgerot et al. (2013)	Sée River	7/05/12	Undular	1.39	3.2	0.4	0.9	14.82	21.7	0.56	1.101	1.060	1.046	1.87	0.014	6.26	1.34
Reungoat et al. (2014a)	Garonne River	7/06/12	Undular (very flat)	*1.02*	*3.85*	0.68	2.72	158.9	79.0	0.45	1.067	1.033	1.043	1.233	--	--	--
		7/06/12	Undular	1.19	4.58	0.59	2.65	152.3	78.7	0.52	1.071	1.032	1.040	1.278	--	--	--
Present study	Garonne River	19/10/13	Undular	1.27	4.32	0.26	2.05	85.6	65.0	0.30	1.031	1.013	1.011	1.231	0.027	2.90	0.96

Notes: A_1: channel cross-section area immediately prior to the bore passage; a_w: wave amplitude of first undulation; B_1: free-surface width immediately prior to the bore passage; d_1: water depth next to ADV immediately prior to the bore passage; F_1: tidal bore Froude number (Eq. (4)); L_w: wave length of first undulation; T_w: period of first undulation; U: tidal bore celerity positive upstream on the channel centreline; V_1: downstream surface velocity on the channel centreline immediately prior to the bore passage; (--): data not available; ***Bold italic data***: incomplete data.

Table 2 - Turbulence properties before and after the tidal bore of the Garonne River on 19 October 2013

Description	Time since 19/10/13 00:00 (s)	$\overline{V_x}$ (m s^{-1})	$\dfrac{v_x'}{\overline{\|V_x\|}}$	$\dfrac{v_y'}{\overline{\|V_x\|}}$	$\dfrac{v_z'}{\overline{\|V_x\|}}$	$\dfrac{v_y'}{v_x'}$	$\dfrac{v_z'}{v_x'}$
(1)	(2)	(3)	(4)	(5)	(6)	(7)	(8)
End ebb tide	61292-61492	+0.109	0.242	0.195	0.120	0.806	0.495
Immediately prior to tidal bore	61492-61512	+0.100	0.191	0.149	0.091	0.779	0.475
Immediately after tidal bore	61522-61542	-0.823	0.089	0.064	0.040	0.723	0.446
Early flood tide	62090-62290	-0.869	0.157	0.112	0.074	0.712	0.472
Mid-flood tide (end of study)	65600-65800	-1.162	0.066	0.042	0.025	0.639	0.384

Note: V_x: longitudinal velocity positive downstream.

Table 3 - Integral turbulent time scales before and after the tidal bore on 19 October 2013

Description	Time since 19/10/13 00:00 (s)	$\overline{V_x}$ (m s^{-1})	T_{Vx} (s)	T_{Vy} (s)	T_{Vz} (s)
(1)	(2)	(3)	(4)	(5)	(6)
End ebb tide	61292-61492	+0.109	0.973	0.384	0.375
Early flood tide	62090-62290	-0.869	9.436	4.336	0.872
Mid-flood tide (end of study)	65600-65800	-1.162	10.38	0.468	0.840

(a) Bore entering the Arcins Channel on 19 October 2013 - The Arcins Island is on the left of the photograph - Note the Airbus barge in the background travelling upstream behind the tidal bore

(b) Bore at Podensac on 24 August 2013, 26 km upstream of Arcins
Fig. 1 - Tidal bore of the Garonne River (France), looking downstream
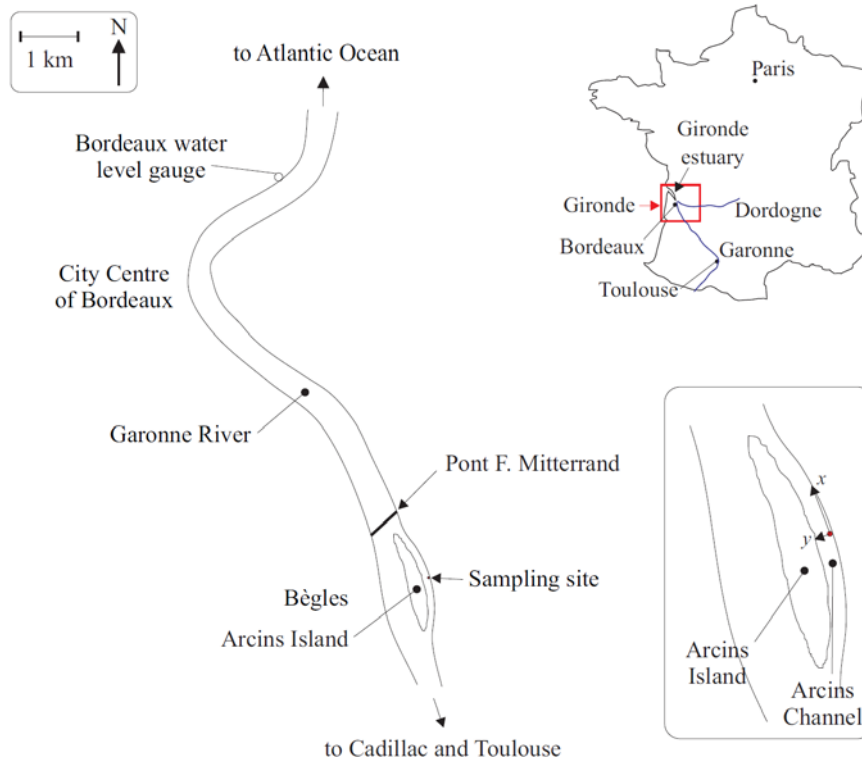
(a) Sketch of Garonne River and Arcins Island (inset: Map of France and coordinate system in the Arcins Channel)
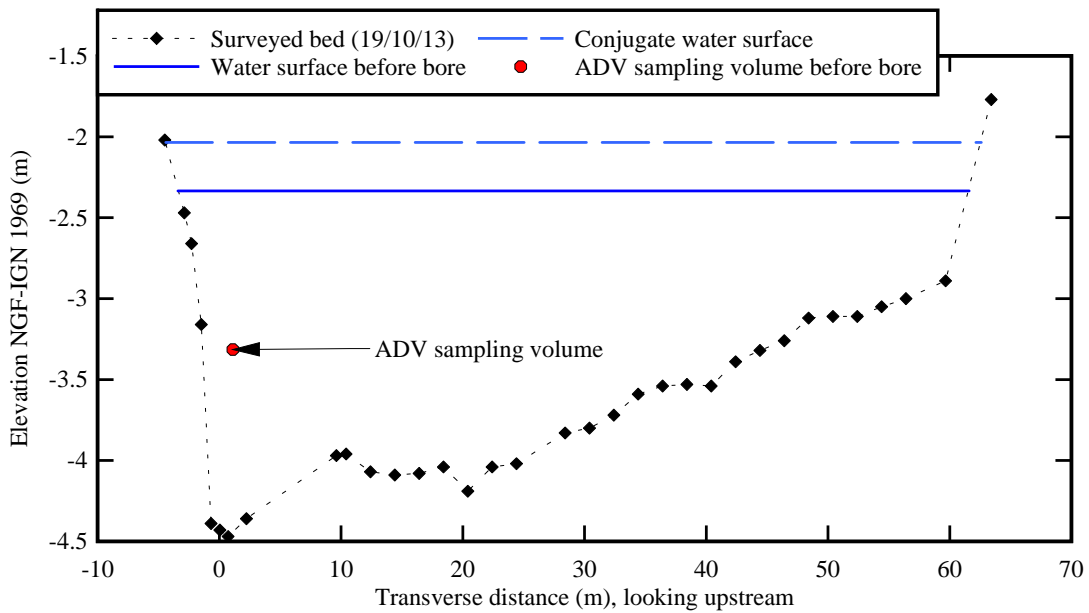
(b) Surveyed cross-section of the Arcins Channel on 19 October 2013 at the sampling site, looking upstream (i.e. South) - Water levels immediately before and after bore front are shown for 19 October 2013, as well as ADV sampling volume location prior to the bore arrival

Fig. 2 - Sampling site
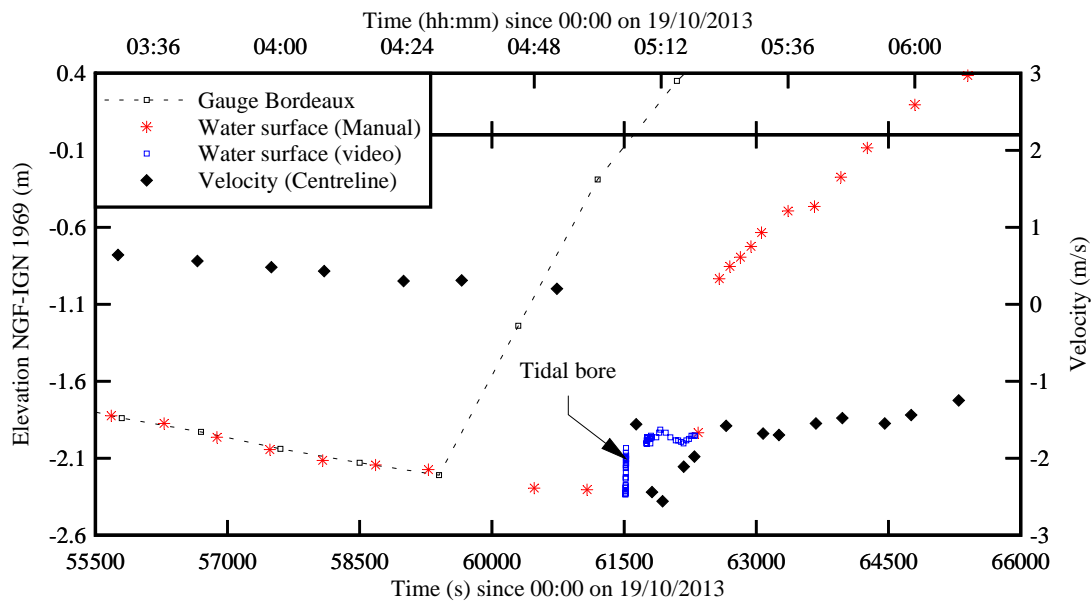
Fig. 3 - Time variations of the water surface elevation next to the ADV unit and free-surface velocity at the channel centre - Comparison with the measured water elevations at Bordeaux (44°52'N, 0°33'W), 10 km downstream of the Arcins Channel (Data: Vigicrue, Ministère de l'Environnement et du Développement Durable)
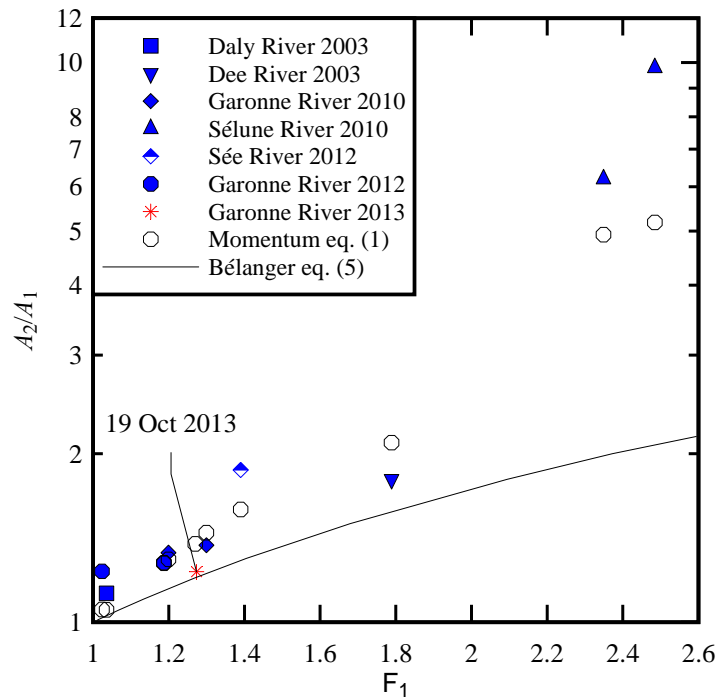
Fig. 4 - Relationship between the conjugate cross-sectional area ratio A_2/A_1 and Froude number F_1 for tidal bore field observations - Comparison with the momentum principle (Eq. (1)) and the classical Bélanger equation (5)
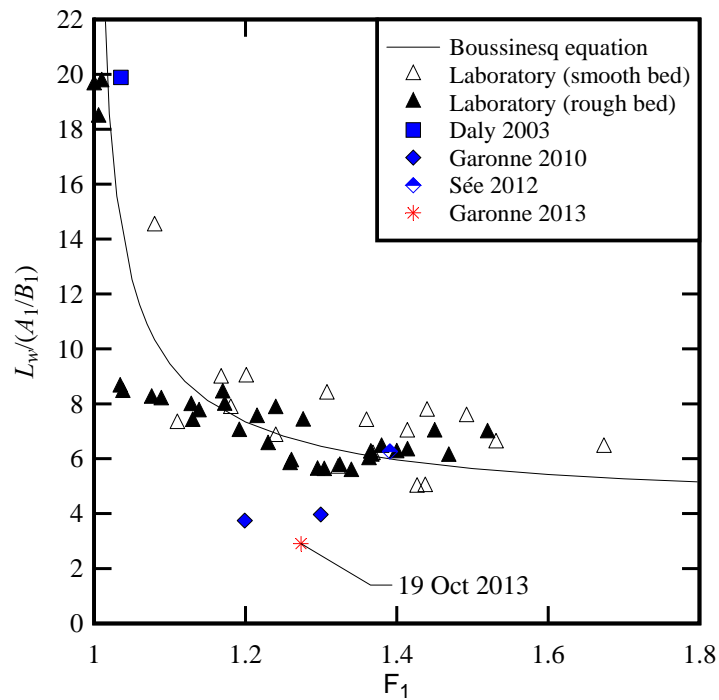
(a) Dimensionless wave length
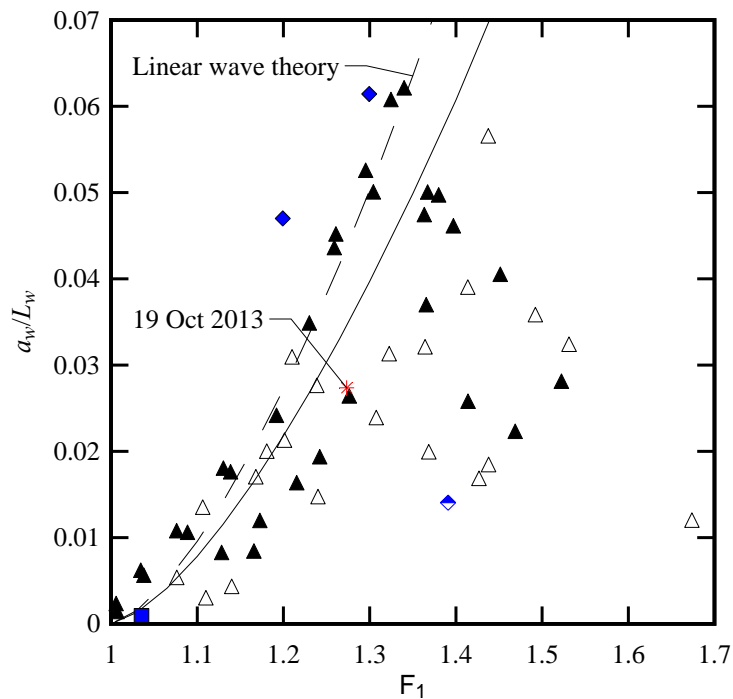
(b) Wave steepness

Fig. 5 - Free-surface undulation properties in tidal bores - Comparison with laboratory data, linear wave theory (dashed line) and Boussinesq equation solution (solid line) - Same legend for both graphs
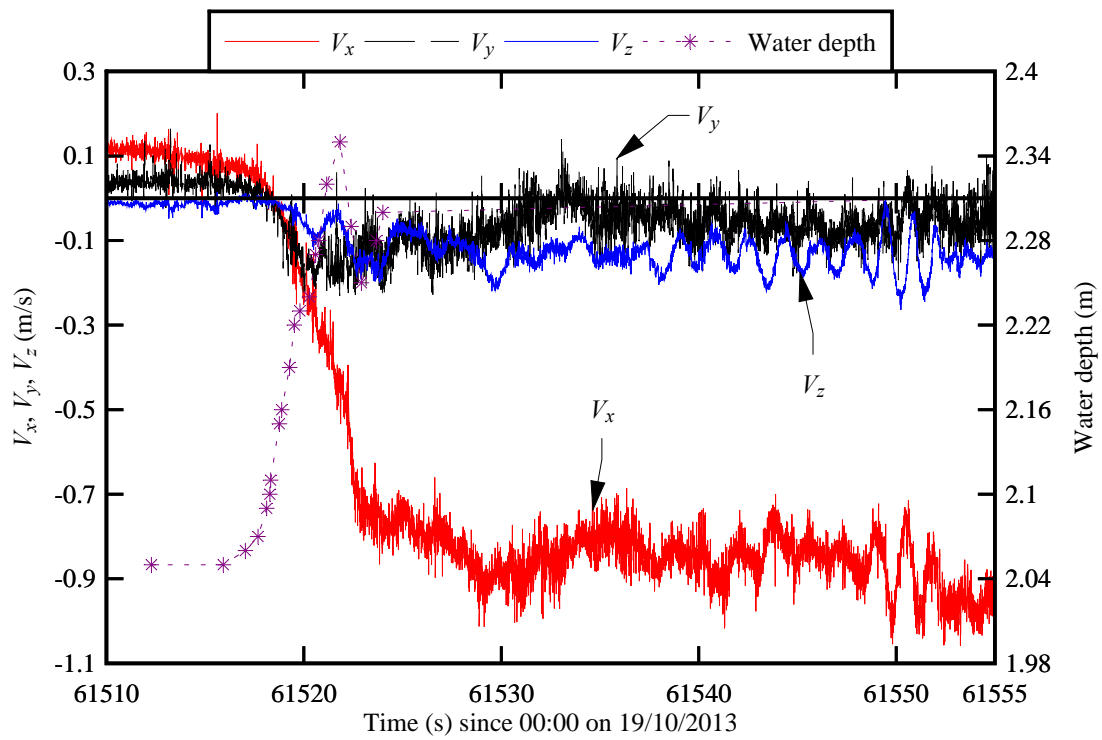
Fig. 6 - Instantaneous velocity components and water depth as functions of time during the tidal bore passage on 19 October 2013
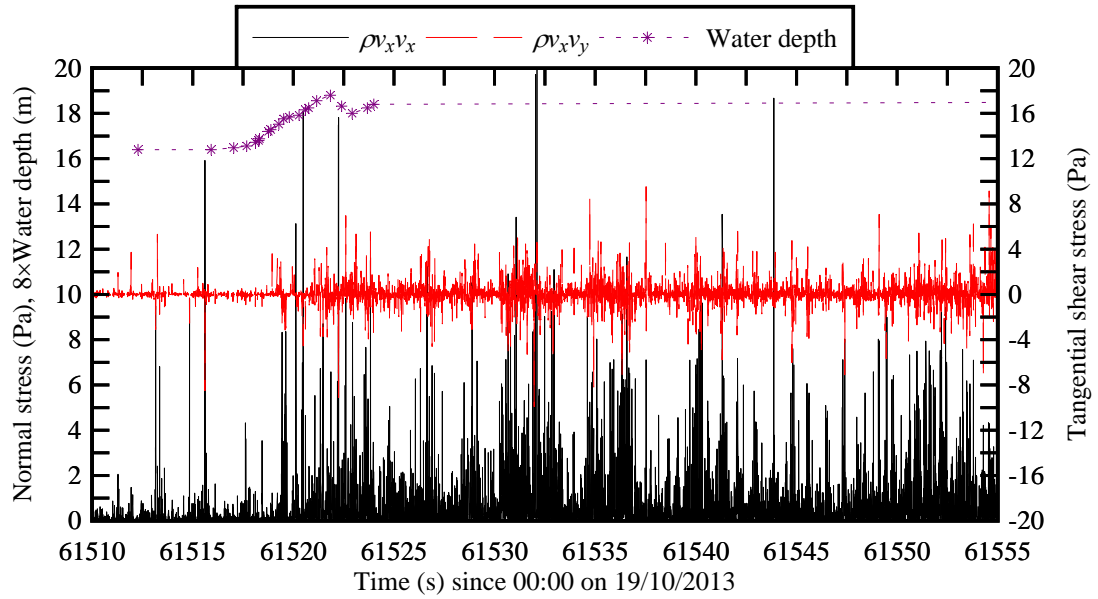
(a) ρv_x^2 and $\rho v_x v_y$
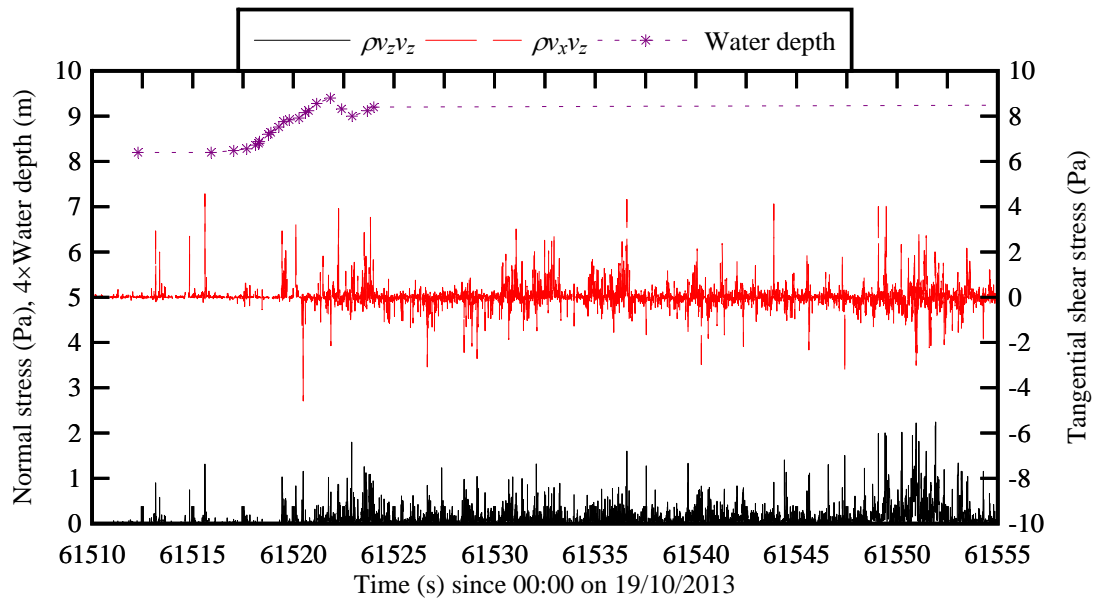
(b) ρv_z^2 and $\rho v_x v_z$

Fig. 7 - Instantaneous Reynolds stress tensor components and water depth as functions of time during the tidal bore passage on 19 October 2013
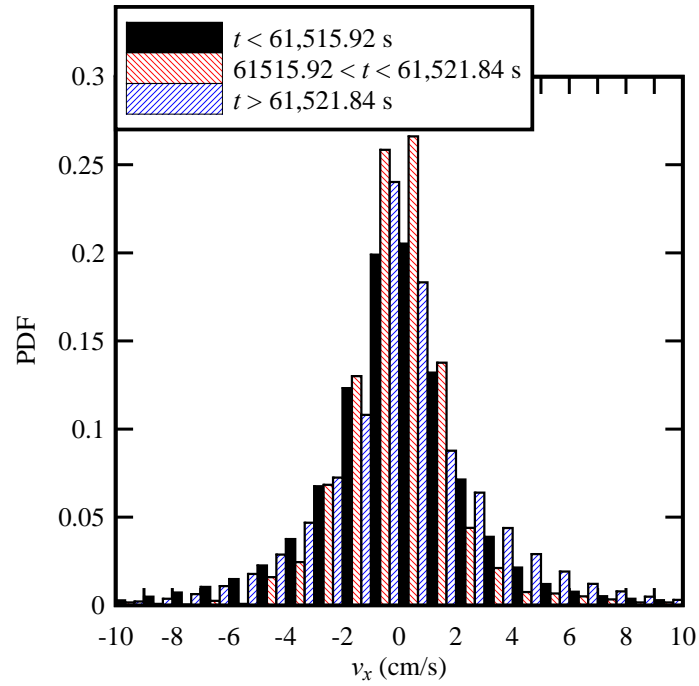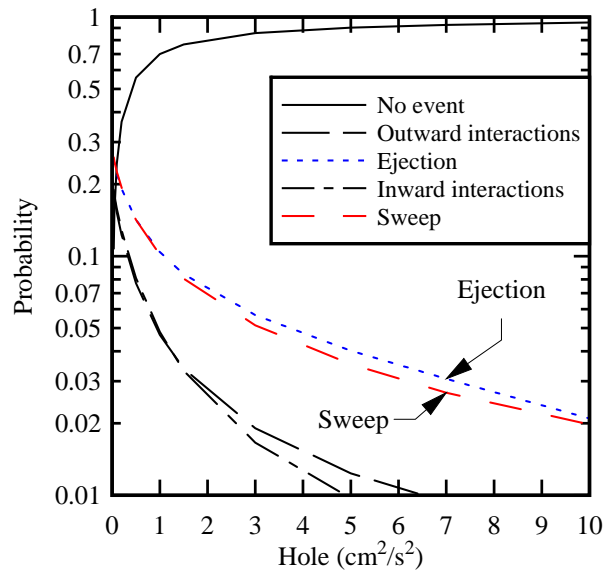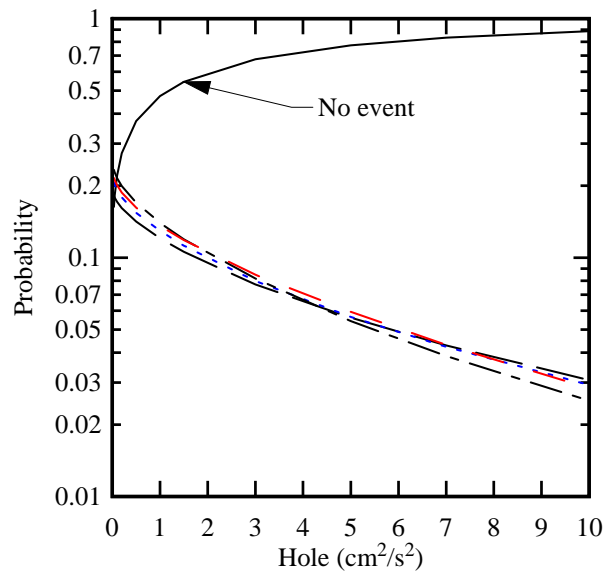
Fig. 8 - Probability distribution function of longitudinal velocity fluctuations v_x during the late ebb tide, bore passage and early flood tide on 19 October 2013

(a) During the late ebb tide ($58000 < t < 61515.92$ s)

(b) During the early flood tide ($61521.84 < t < 63000$ s)

Fig. 9 - Fraction of time of Reynolds stress $v_x v_z$ during the late ebb tide and early flood tide on 19 October 2013 (Same legend for both graphs)